

Consideration of memory of spin and parity in the fissioning compound nucleus by applying the Hauser-Feshbach fission fragment decay model to photonuclear reactions

T. Kawano,^{1,*} A. E. Lovell,¹ S. Okumura,² H. Sasaki,¹ I. Stetcu,¹ and P. Talou¹

¹*Los Alamos National Laboratory, Los Alamos, NM 87545, USA*

²*NAPC-Nuclear Data Section, International Atomic Energy Agency, Vienna A-1400, Austria*

(Dated: December 20, 2022)

Prompt and β -delayed fission observables, such as the average number of prompt and delayed neutrons, the independent and cumulative fission product yields, and the prompt γ -ray energy spectra for the photonuclear reactions on $^{235,238}\text{U}$ and ^{239}Pu are calculated with the Hauser-Feshbach Fission Fragment Decay (HF³D) model and compared with available experimental data. In the analysis of neutron-induced fission reactions to the case of photo-induced fission, an excellent reproduction of the delayed neutron yields supports a traditional assumption that the photo-fission might be similar to the neutron-induced fission at the same excitation energies regardless of the spin and parity of the fissioning systems.

PACS numbers: 24.60.-k, 24.60.Dr

I. INTRODUCTION

Nuclear fission phenomena have been studied in the three distinct reaction time domains, namely in the dynamical evolution of compound nucleus before scission, during the statistical decay of highly-excited fission fragments, and following the β -decay of produced fission products after prompt emission of neutrons and γ rays. The neutrons and γ rays emitted from the fission fragments give particularly important traces to understand this complicated process as a whole, as the emission of these particles is governed by the strict spin, parity, and energy conservation rules during the sequence of fission fragment decay. How the compound nucleus in a compact configuration splits into two correlated objects, where the total fission energy is transferred into the excitation energies of both fragments as well as the kinetic energy of their relative motion, is one of the common questions in nuclear fission.

Total spin J of the fissioning compound nucleus formed by a neutron-induced reaction is restricted to $\mathbf{J} = \mathbf{I} + \mathbf{j}$, where I is the target nucleus spin and j is the total spin of the neutron. For example, a thermal-neutron-induced reaction on ^{235}U (ground state spin of $7/2^-$) produces the compound states of $J = 3^-$ and 4^- only. In contrast to this limited range of J , a much wider distribution of angular momenta in the formed fragments is often advocated for by both experimental and theoretical studies [1–9] at the moment of scission. A simple and classical picture of the origin of the high spin is the torque produced by strong Coulomb repulsion between the formed fragments, and this repulsion may strongly depend on the configuration of two compound nuclei in the vicinity of the scission. We may deductively infer the configuration of fission fragments by measuring the characteristics of the emitted neutrons and/or γ rays and

comparing them with predictions from recent fission fragment decay models [10–17], where the statistical Hauser-Feshbach theory [18] ensures the spin-parity conservation at each stage of the fission fragment decay.

Recently, the Hauser-Feshbach Fission Fragment Decay (HF³D) model has been successfully applied to neutron-induced fission reactions [16, 17, 19], including both prompt and delayed particle emissions. Although the model depends on some phenomenological parameters that are often determined by experimental data such as the initial mass and kinetic energy distributions of the primary fission fragments, essential properties of the compound nucleus just after the scission can be studied. The HF³D model has been applied to neutron-induced reactions, as it allows us to calculate fission observables in a system-energy-dependent way. Photonuclear fission is an alternative approach to study fission process [20], where the electric and magnetic transitions populate selective spin states in the compound nucleus, different from those populated in (n, f) reactions. By comparing the neutron and photo-induced fission reactions, we may investigate if information of the spin of the fissioning compound nucleus is transmitted to the two fission fragments beyond the sudden transition from one-body compound nucleus. In first-order approximation, we assume that the photo-nuclear reaction occurring on the target nucleus (Z, A) at the γ -ray energy of E_γ is equivalent to the neutron-induced case on $(Z, A-1)$ at $E_n = E_\gamma - S_n$, where S_n is the neutron separation energy. We expect that difference in the spin distribution of the compound system will impact some correlation observables, although it will be minimal for average quantities like average multiplicities of prompt particles, and so on. In this paper, we provide HF³D analyses for the γ -ray induced reactions on the major actinides and discuss the difference and similarity between the γ -ray and neutron induced reactions. The HF³D model calculation is performed with the BEOH module, which is part of the statistical Hauser-Feshbach nuclear reaction code COH₃ [21]. Instead of performing the com-

* kawano@lanl.gov

pound nucleus decay by applying the Monte Carlo technique [10, 11, 13, 15], BEOH numerically integrates the distributions of fission fragment yields, spin, parity, and excitation energy to produce precise fission observables even when extremely small fission fragment yields are expected.

II. THEORY

A. Spin and parity population in compound nucleus

The photo-nuclear reaction populates limited space in the spin and parity states in a compound nucleus. In the giant dipole resonance (GDR) region (typically around ~ 10 MeV for heavy nuclei), the E1 transition is the dominant contribution to the absorption of incident γ rays, which populates $I \pm 1$ states with flipped parity. The M1 transition, which also populates the $I \pm 1$ states but with the same parity, is generally weaker in the GDR region. However, near the neutron separation energy (~ 5 MeV), M1 can be comparable for the deformed systems [22–24]. In contrast, the neutron-induced reactions in the same energy range lead to wider spin and parity space in the formed compound nucleus, as the incident neutron can bring more orbital momenta into the compound.

To illustrate the difference in the populated spin and parity in the fissioning compound nucleus, we calculate the partial populations for each J^Π to the total compound formation cross section. The partial compound formation cross section that produces the J^Π state is

$$\sigma(J, \Pi, E) = \frac{\pi}{k^2} g_J \sum_{lj} T_{lj}(E), \quad (1)$$

where g_J is the spin factor, k is the incoming particle wave number, and T_{lj} is the transmission coefficient for the orbital angular momentum l and the total spin j . The coupling scheme is $\mathbf{J} = \mathbf{I} + \mathbf{j}$, and we omit trivial parity conservation here. The total compound formation is

$$\sigma(E) = \sum_{J^\Pi} \sigma(J, \Pi, E), \quad (2)$$

and the partial contribution is defined as

$$P(E, J, \Pi) = \frac{\sigma(J, \Pi, E)}{\sigma(E)}. \quad (3)$$

For neutron-induced reactions, the partial population is calculated from the optical model transmission coefficients. Here we adopt the coupled-channels optical potential of Soukhovitskii et al. [25]. For the γ -ray incident reactions, they correspond to the partial contributions from the E1 and M1 transitions. The photo-absorption cross section can be calculated by the Quasi-particle Random Phase Approximation (QRPA), and we applies

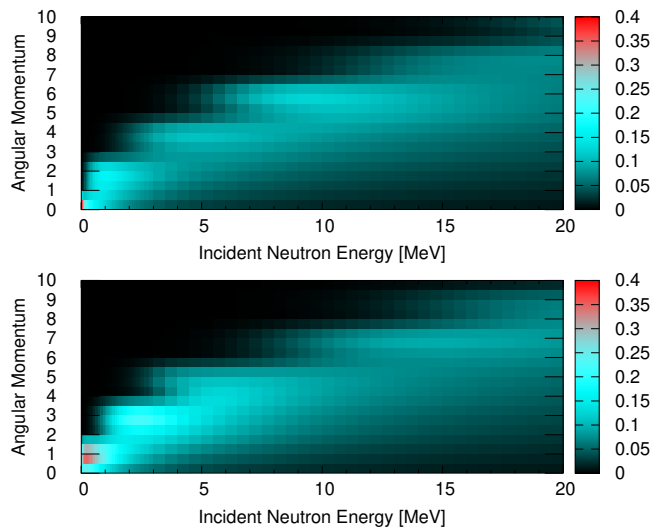


FIG. 1. Partial population of compound nucleus for the neutron-induced reaction on ^{238}U as a function of neutron energy. The top panel is for the even parity and the bottom is for the odd parity.

the non-iterative Finite Amplitude Method (FAM) [26–28] based on the Hartree-Fock-BCS theory [29] to solve QRPA equations. From the partial component of photo-absorption cross section $\sigma_{XL}(E)$, where $X = \text{E or M}$ is the type of interaction, and the multipolarity $L = 1$ for the E1 and M1 transitions, the γ -ray transmission coefficient T_{XL} is given by

$$T_{XL}(E) = \frac{2}{2l+1} \left(\frac{E}{\hbar c} \right)^2 \sigma_{XL}(E). \quad (4)$$

By substituting T_{XL} into Eq. (1) as $T_{lj} = T_{LL}$ with a proper parity conservation for the E and M transitions, $P(J, \Pi)$ is also calculated in the photo-nuclear reaction case.

Figures 1 and 2 are the calculated partial populations with the coupled-channels optical model and the γ -ray strength function for the target nucleus of ^{238}U . Obviously the compound states formed by a neutron distribute over a few \hbar width in the GDR region, while 1^\pm states are selectively populated by the γ ray incident. An even-odd parity wiggle seen in the population below 5 MeV is due to competing E1 and M1 transitions, which is also seen in the microscopic calculations [28].

The population by a γ ray can also be estimated by adopting global parameterization of E1 and M1, such as the generalized Lorentzian proposed by Kopecky and Uhl [30] with the systematic study of M1 scissors mode [24]. The result shows much less parity fluctuation in $P(J, \Pi)$ compared to the QRPA case.

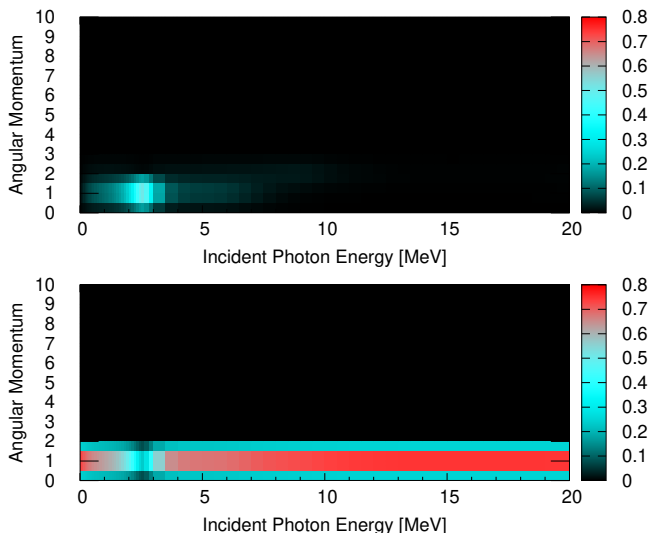


FIG. 2. The same as Fig. 1 but for the photo-induced reaction calculated with the QRPA method.

B. Hauser-Feshbach decay of fission fragments

We assume that the two fragments produced by fission are fully equilibrated compound nuclei after they are well separated from Coulomb repulsion. These fragments tend to be highly excited and have high angular momenta. The HF³D model replaces the compound nucleus decay width by the optical model transmission coefficients in the inverse reaction channel, as proposed by Hauser and Feshbach [18], and the prompt fission observables are well characterized once the initial configuration of the fission fragments is specified. Since the details of HF³D model are discussed elsewhere [14, 16, 17], here we briefly give an overview of this model. Although we deal with the photo-induced fission in this study, the formulae are common unless specified otherwise.

First, we define an initial population $P_{L,H}(E_x, J, \Pi)$ in a compound nucleus, where the subscript L, H stands for the light and heavy fragments. The initial population is a joint distribution of excitation energy $G_{L,H}(E_x)$, spin $R_{L,H}(J)$, and parity $P(\Pi)$. The population is normalized as

$$\sum_{J\Pi} \int P_{L,H}(E_x, J, \Pi) dE_x = 1. \quad (5)$$

We assume the excitation energy distribution is described by Gaussian. The spin distribution follows the shape given by the Gilbert-Cameron level density formula [31, 32], but the spin-cutoff parameter σ^2 is scaled by an adjustable parameter f_J

$$R_{L,H}(J) = \frac{J + 1/2}{(f_J \sigma_{L,H})^2} \exp \left\{ -\frac{(J + 1/2)^2}{2(f_J \sigma_{L,H})^2} \right\}, \quad (6)$$

to take the high spin population in the fission into account. $R(J)$ satisfies the normalization condition of

$\sum_J R(J) = 1$. An equal distribution is assumed for the parity distribution.

Second, the total excitation energy E of the system is restricted by the Q -value of splitting the fissioning compound nucleus (Z_{CN}, A_{CN}) into the fragments (Z_L, A_L) and (Z_H, A_H), as well as the total kinetic energy T taken by the acceleration of fragments. A simple linear dependence on the incident energy is assumed for the average total kinetic energy

$$T(E) = T_0 + T_1 E_\gamma, \quad (7)$$

where E_γ is the incident γ -ray energy, and the constant T_0 is often taken from a systematic study by Viola [33], and tuned as necessary. The total excitation energy is divided into the excitation energy of both the fission fragments by the so-called R_T model [10, 34], and the distribution width is also determined by the dispersion of T and the kinematics [14], the initial population $P_{L,H}(E_x, J, \Pi)$ is thus characterized.

Finally, the aggregation calculation for all the fission fragment pairs requires distributions of mass and charge numbers. The mass distribution is modeled by the five Gaussian shapes,

$$Y_P(A) = \sum_{i=1}^5 \frac{F_i}{\sqrt{2\pi}\sigma_i} \exp \left\{ -\frac{(A - A_m + \Delta_i)^2}{2\sigma_i^2} \right\}, \quad (8)$$

where σ_i and Δ_i are the Gaussian parameters, $A_m = A_{CN}/2$ is the mid-point of the mass distribution, and F_i is the fraction of each Gaussian component. We employ Wahl's Z_p model [35, 36] for the charge distribution. Because Wahl's parameterization of the even-odd term in the Z_p model is often unsatisfactory to reproduce the delayed neutron yield [17, 37], we introduce rescaling factors of f_Z and f_N to reinforce the even-odd effect

$$F_Z = 1.0 + (F_Z^W - 1.0)f_Z, \quad (9)$$

$$F_N = 1.0 + (F_N^W - 1.0)f_N, \quad (10)$$

where F_Z^W and F_N^W are defined in the original Z_p model.

C. Model parameters for photo-induced fission

We have obtained sets of the HF³D parameters for major actinides (^{235,238}U and ²³⁹Pu) in our past study [17], for the neutron-induced fission reactions up to the second chance fission threshold. The multi-chance fission parameters for ²³⁵U were also reported by Lovell *et al.* [16]. Here we employ the model parameters obtained by Okumura *et al.* [17], and extend them to the multi-chance fission calculations for consistency.

Because the mass distribution of Eq. (8) is defined as a relative mass to A_m , these distributions can be applied to each fission chance by shifting A_m , *e.g.* $A_m = 117.5$ for the first chance of photo-induced fission on ²³⁵U, 117 for the second chance, *etc.* We assume the Gaussian fractions F_i for the photo-induced fission are the same for

the neutron-induced fission on the same target, but they are corrected by the neutron separation energy. We further assume that R_T , f_J , f_Z , and f_N are the same as the neutron-induced case. Therefore, the main difference between the neutron and photo-induced reactions is the total kinetic energy. Although we are able to adopt the same values as the neutron-induced data analysis, our preliminary study showed that the calculated average number of prompt neutrons $\bar{\nu}_p$ deviates significantly from the experimental data. Hence, we readjust T to the experimental $\bar{\nu}_p$ in the next section.

D. Fission observables

The HF³D model produces several fission observables simultaneously, such as the average number of prompt neutrons $\bar{\nu}_p$, the average number of emitted neutrons for each fragment mass $\bar{\nu}(A)$, the prompt fission neutron and γ -ray spectra, and the independent fission product yields $Y_I(Z, A)$, and so on. By providing the decay data of fission products, the model also produces the average number of delayed neutrons $\bar{\nu}_d$ and the cumulative fission product yields $Y_C(Z, A)$. We take the evaluated decay data of ENDF/B-VIII.0 [38] for calculating the β -delayed components.

Since the HF³D model has been extended to the multi-chance fission [16], in which a few pre-fission neutrons remove part of total excitation energy, all of the calculated quantities are incident energy dependent. We calculate these fission observables up to 20 MeV γ -ray incident energy, where the typical observed data are a convolution of (γ, f) , (γ, nf) , $(\gamma, 2nf)$, and $(\gamma, 3nf)$ reactions.

III. RESULTS AND DISCUSSION

A. Average number of prompt neutrons

The average number of prompt neutrons $\bar{\nu}_p$ is sensitive to the available excitation energies in the light and heavy fragments, and therefore, it depends on the total kinetic energy, T . Experimental energy dependence of T for major actinides often shows a negative slope [39–43] except for a somewhat flattened behavior observed at very low energies [44, 45]. The linear parameters T_0 and T_1 in Eq. (7) are adjusted to reproduce the experimental $\bar{\nu}_p$ of the photo-induced reactions on ^{235,238}U and ²³⁹Pu. The calculated $\bar{\nu}_p$'s are compared with experimental data [20, 46–51] in Fig. 3, as well as the evaluated data in the IAEA photonuclear data library 2019 [52]. The IAEA data are identical to the JENDL photonuclear data file [53] in this energy range. The obtained parameters are tabulated in Table I, and compared with the systematics of Viola [33]. The obtained parameters for ^{235,238}U agree fairly well with Viola, while our ²³⁹Pu is 5.4 MeV higher. This is due to a smaller f_J parameter of 1.58 for ²³⁹Pu than 2.96 for ^{235,238}U in Ref. [17].

The f_J parameter and T are anti-correlated and different estimates of f_J and T may give similar results. By comparing to the Viola systematics, a higher f_J might be favorable, nevertheless a definitive conclusion cannot be cast at this point due to the limited experimental information as well as the compensation error between f_J and T .

In our past analysis of neutron-induced fission [14], the total kinetic energy for ²³⁵U is estimated to be $T = 171.2 - 0.18E_n$ MeV. By shifting the neutron separation energy of 5.298 MeV and assuming T weakly depends on the mass, 170.3 MeV is 0.7% lower than the obtained T of 171.5 MeV. Although data fitting is not an objective of this study, such a difference might be compensated by re-adjusting f_J to obtain the similar quality of fit to $\bar{\nu}_p$, since f_J changes the competition of neutron and γ -ray emission. However, in such a case a survey of the experimental data on prompt γ emission would be in order.

Experimental total kinetic energy data are generally not mono-energetic. De Clercq et al. [54] reported measurements of the total kinetic energy with the bremsstrahlung γ -ray source that has the maximum γ -ray energy of 25 MeV. Their data are 170.6 ± 2 MeV for ²³⁵U and 170.9 ± 2 MeV for ²³⁸U. The multi-chance fission probability weighted average of values in Table I are 169.7 MeV and 171.1 MeV for ²³⁵U and ²³⁸U, which agree with the experimental data.

The HF³D results slightly deviate from the linear function as assumed in the IAEA/JENDL evaluations, and this is mainly due to the multi-chance fission effect. As demonstrated by Lovell *et al.* [16], fission occurs at relatively low excitation energy due to the multi-chance fission even though the incident particle brings large energies into the system, and $\bar{\nu}_p$ is determined by the main fissioning compound nucleus in each multi-chance fission realm.

Note that although we calculate photo-induced reactions for low energy photons as well, they are often below the fission barriers and these calculated yields are understood to be for the sub-threshold fission. In addition to the fact the photo-absorption cross section at a few MeV is very small, they are hardly observed experimentally.

B. Prompt γ -ray energy spectra

Many prominent discrete prompt fission γ -ray lines are seen in the energy spectra, which are produced by the discrete γ -ray transitions in the fission products shortly after scission, or slightly delayed due to the isomer production [55, 56]. We aggregate the discrete γ rays separately then add them to the continuum spectrum using 10-keV energy bins. This width roughly corresponds to the Doppler effect caused by the moving fission fragments. The calculated γ -ray energy spectra for selected incident γ -ray energies are shown in Fig. 4 up to 2 MeV. Sometimes a peak in the spectrum is produced by a single

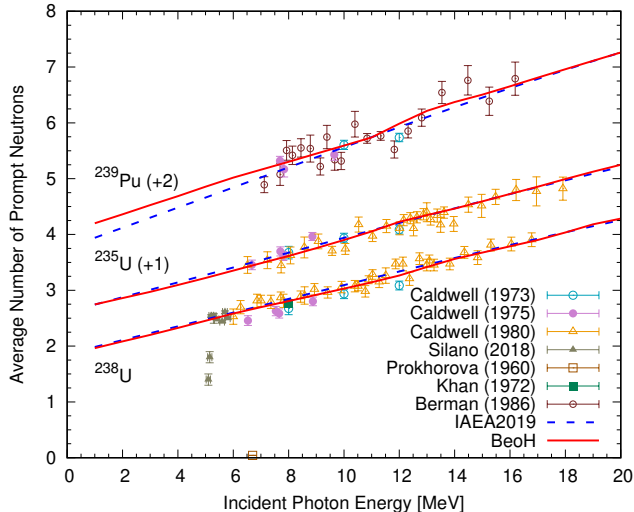


FIG. 3. The calculated average number of prompt neutrons $\bar{\nu}_p$ as functions of incident γ -ray energy compared with the available experimental data [20, 46–51]. The comparisons for ^{235}U and ^{239}Pu are shifted by +1 and +2. The dashed lines are the evaluated $\bar{\nu}_p$ in the IAEA photonuclear data library 2019 [52].

TABLE I. The estimated total kinetic energies for the photo-fission of $^{235,238}\text{U}$ and ^{239}Pu , which are expressed as $T = T_0 + T_1 E_\gamma$, where E_γ is in MeV. They are also compared with the systematics of Viola [33].

Target	CN	T_0 [MeV]	T_1 Viola [MeV]
^{235}U	^{235}U	171.5	-0.10
	^{234}U	171.6	-0.10
	^{233}U	170.6	-0.20
^{238}U	^{238}U	171.1	-0.05
	^{237}U	171.9	-0.05
	^{236}U	172.8	-0.05
	^{239}Pu	182.0	-0.42
^{239}Pu	^{238}Pu	179.0	-0.42
	^{237}Pu	177.1	-0.20

discrete transition, while one histogram bin may include a few γ lines in many cases. The calculated spectra extend to more than 20 MeV, which is also observed in the thermal-neutron-induced fission case [57]. Their shapes all resemble one another and are less informative, hence we show the spectra at the 10 MeV case in Fig. 5. We also compare these spectra with the case of thermal-neutron-induced fission on ^{235}U , where the model parameters are the same as those by Okumura *et al.* [17].

C. Cumulative fission product yields

The experimental data of cumulative fission product yields, $Y_C(Z, A)$, for photo-fission reactions are rather in-

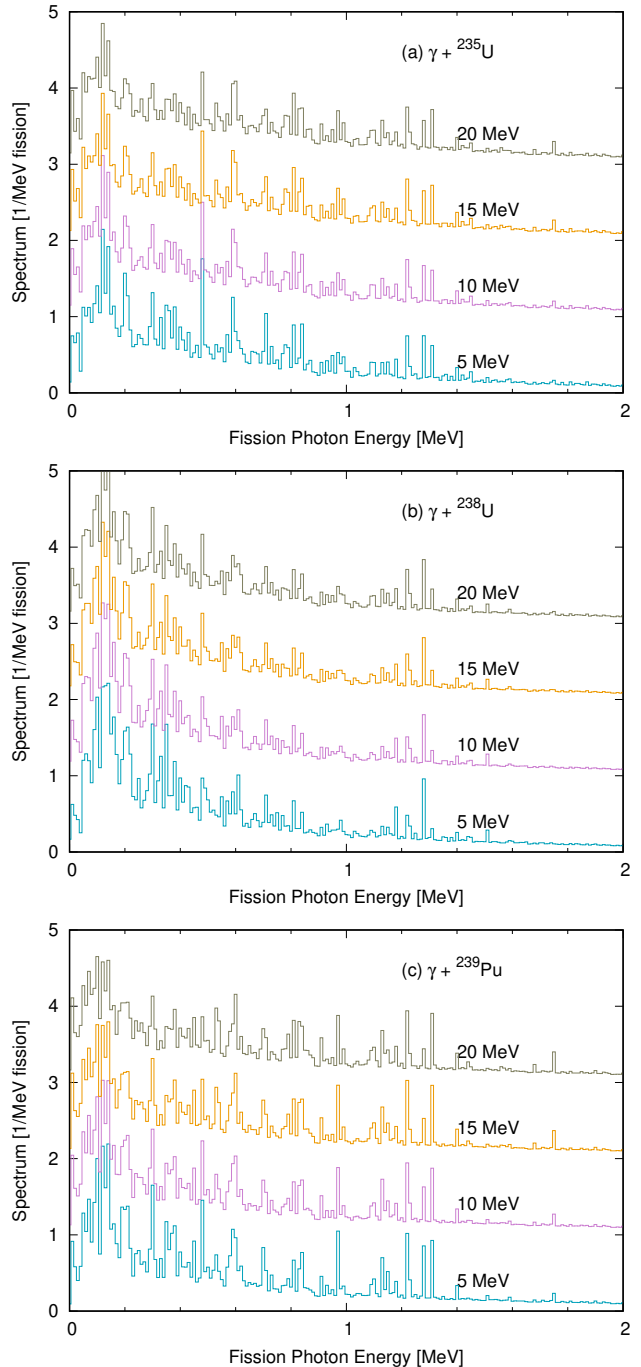


FIG. 4. The calculated prompt fission γ -ray spectra for the photo-fission on $^{235,238}\text{U}$ and ^{239}Pu at 5, 10, 15, and 20 MeV.

accessible. Krishichayan *et al.* [58] reported 37 $Y_C(Z, A)$ data for $\gamma+^{235}\text{U}$ and 36 for $\gamma+^{238}\text{U}$ at 13 MeV those are measured with the mono-energetic photon beam at the HI γ S facility. We compare our calculated results with the data of Krishichayan *et al.* [58] in Fig. 6. Here we do not specify the atomic numbers for the sake of simplicity. Each of the calculated point corresponds to those mea-

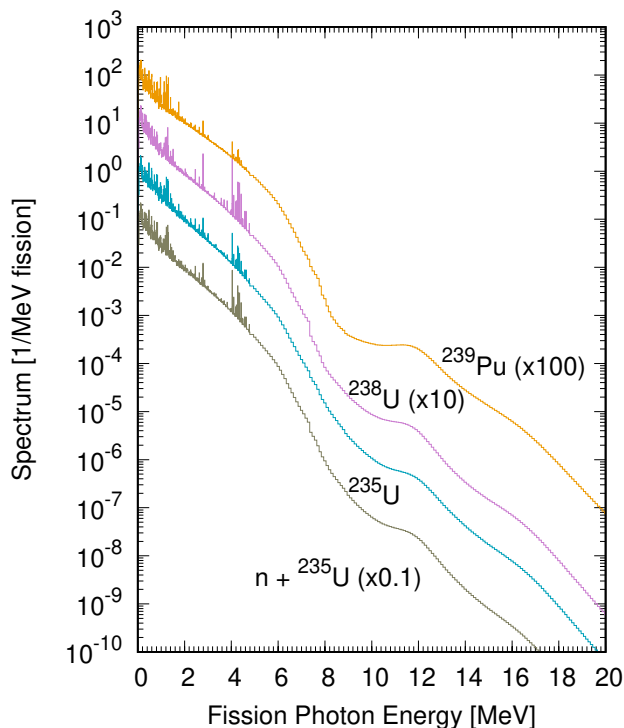


FIG. 5. The calculated prompt fission γ -ray spectra for the photo-fission on $^{235,238}\text{U}$ and ^{239}Pu at 10 MeV. The bottom curve is for the case of thermal-neutron induced fission on ^{235}U .

sured values. The calculated $Y_C(Z, A)$ for ^{235}U agrees with the data reasonably well, while the case of ^{238}U has a large deviation in the mass range 90 – 95. We cannot reproduce such high $Y_C(Z, A)$ without maintaining rather good fit to the data in the heavy mass range.

Thierens *et al.* [59] measured the cumulative mass yields by the bremsstrahlung photon source that has the maximum energy of 25 MeV. Since an exact photon energy spectrum for this measurement is unknown, we average our calculated results with the weighting factor of $w(E_\gamma) = c\sigma_f(E_\gamma)/E_\gamma$, where σ_f is the evaluated photo-fission cross section in the IAEA photonuclear data library, and c is a normalization factor. Although this would not be an exact comparison because of an uncertain photon energy spectrum at the sample location, Fig. 7 compares the energy-averaged mass yield

$$\bar{Y}_C(A) = \int \sum_Z w(E_\gamma) Y_C(Z, A, E_\gamma) dE_\gamma, \quad (11)$$

which seems to be in reasonable agreement except for the symmetric region, even though the extension of the calculation to 25 MeV is a rather long-range extrapolation. For better reproduction of the experimental data, we may need steeper energy dependence of the symmetric fission component.

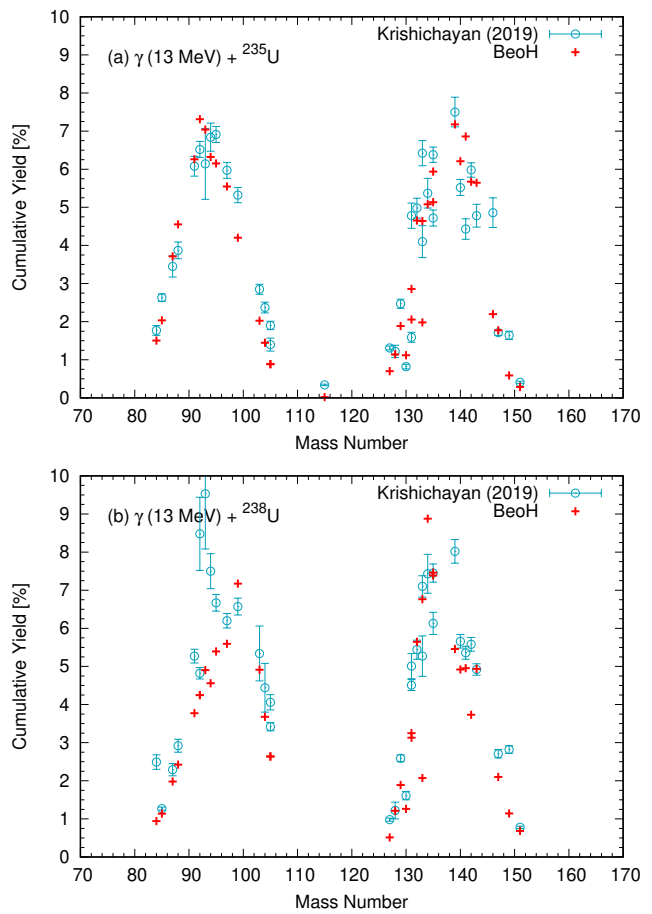


FIG. 6. Calculated cumulative fission product yields at $E_\gamma = 13$ MeV compared with the experimental data of Krishichayan *et al.* Krishichayan *et al.* [58]. The top panel (a) is for ^{235}U , and the bottom (b) is ^{238}U .

D. Average number of delayed neutrons

The average number of delayed neutrons, $\bar{\nu}_d$, is another important quantity to validate the calculated $Y_C(Z, A)$. When a β -decay branch of the precursor (Z, A) includes a delayed neutron emission mode, the delayed neutron yield from this precursor is calculated as $Y_C(Z, A)bN_d$, where b is the branching ratio to the neutron-decay mode, and N_d is usually unity unless multiple neutron emission is allowed. The total delayed neutron yield is thus $\bar{\nu}_d = \sum Y_C(Z, A)bN_d$, and the summation is performed on all the delayed neutron emitters. There are about 200 – 300 delayed neutron emitters included in this study.

The calculated $\bar{\nu}_d$ is shown in Fig. 8 as a function of the incident γ -ray energy, where the agreement with the experimental data [46–48, 60, 61] is rather remarkable. It should be emphasized that the calculated $\bar{\nu}_d$ was not fitted to these data, but they were just consequences of model calculations that are based on the neutron-induced fission as well as the total kinetic energies estimated from

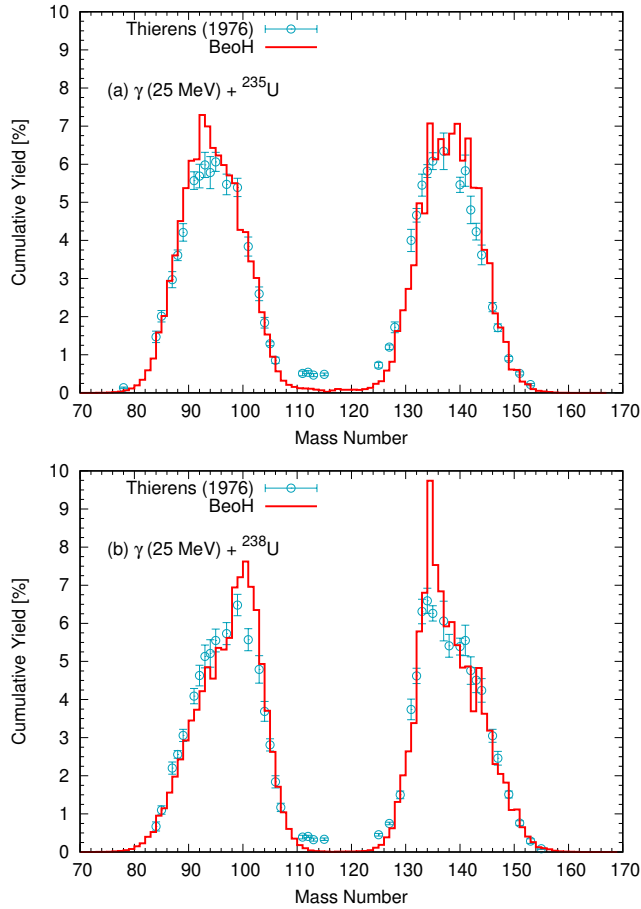


FIG. 7. Calculated cumulative fission product yields averaged over an estimated bremsstrahlung photon energy spectrum that has the maximum energy of $E_\gamma = 25$ MeV compared with the bremsstrahlung data of Thierens *et al.* [59]. The top panel (a) is for ^{235}U , and the bottom (b) is ^{238}U .

the average prompt neutrons $\bar{\nu}_p$. We also plot the evaluated $\bar{\nu}_d$'s in the IAEA photonuclear data library in the same figure, which is again the same as JENDL Photonuclear data file [53]. It is unclear whether this evaluation comes from a fit directly to the experimental data or from a simple functional form. On the contrary, our calculations well reproduce the data without any further adjustments. Notable structure in the calculated $\bar{\nu}_d$ is seen near 11 and 17 MeV, which is clear evidence of the multi-chance fission effects.

As discussed before, the average prompt neutron multiplicity, $\bar{\nu}_p$, is rather evidence of energy conservation that determines the available excitation energies for prompt particle emissions. Even in the multi-chance fission cases, the energy conservation is still governed by the separation energy of pre-fission neutrons and the average kinetic energy of the emitted pre-fission neutrons. Although we modestly adjusted the total kinetic energy T to reproduce the experimental $\bar{\nu}_p$, the changes in T should be within the experimental uncertainties.

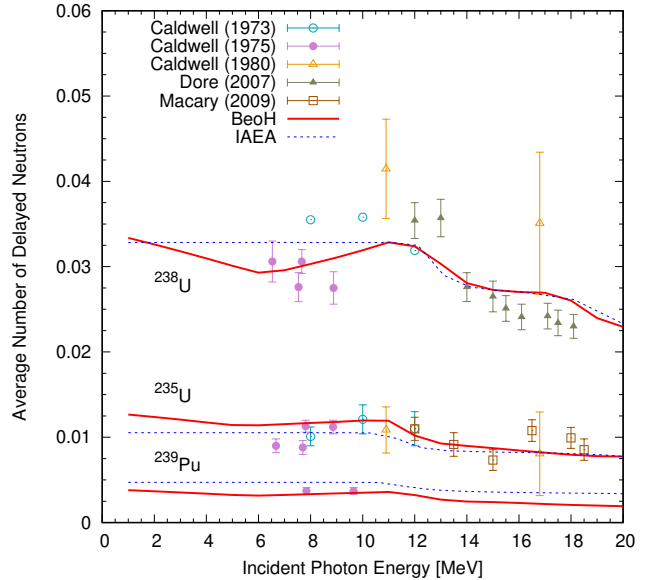


FIG. 8. The calculated average number of delayed neutrons $\bar{\nu}_d$ as functions of incident γ -ray energy compared with the available experimental data [46–48, 60, 61]. The dashed lines are the evaluated $\bar{\nu}_d$ in the IAEA Photonuclear Data Library 2019 [52].

On the other hand, many other factors are involved in the delayed neutron yields, namely the energy dependence of the fission fragment yields $Y_P(A)$, the even-odd effect, and so on. The multi-chance fission probabilities change $\bar{\nu}_d$ significantly, because a shift of one mass unit replaces many of the delayed neutron precursors. As shown in the decent reproduction of $\bar{\nu}_d$ by applying the neutron-induced fission parameters, it is unlikely that the produced fission fragments after scission remember the spin and/or parity of the fissioning system. Our observation supports a traditional assumption that the photo-fission could be approximated by the neutron-induced fission at the same excitation energies. This is in contrast to the very different populations of spin states in the compound nucleus between the neutron and γ -ray induced reactions as shown in Figs. 1 and 2.

IV. CONCLUSION

The spin dependence of the nuclear fission was investigated by applying the statistical Hauser-Feshbach Fission Fragment Decay (HF³D) model to the photo-nuclear reactions on $^{235,238}\text{U}$ and ^{239}Pu . We performed the HF³D model calculations for these targets by employing the model parameters obtained for the neutron-induced fission cases, with re-adjustment of the total kinetic energies to reproduce the average number of prompt fission neutrons. The calculated results were compared with the experimental cumulative fission product yields at mono-

energetic 13 MeV as well as a continuous bremsstrahlung photon source. We also conducted comparisons of the average number of delayed neutrons, obtaining fairly good agreements with the experimental data. While the populated spin and parity states in the fissioning system for the neutron and γ -ray induced reactions are very different, we found that the cumulative fission product yields and the average number of delayed neutrons seem to be insensitive to the spin and parity of the fissioning systems. This observation supports the traditional assumption that the photo-fission might be similar to the neutron-induced fission at the same excitation energies regardless of the quantum numbers of the fissioning systems.

ACKNOWLEDGMENTS

TK thanks to Nobuyuki Iwamoto of JAEA for providing the undocumented information on the JENDL photonuclear data files. He also thanks Anton Tonchev of LLNL, Matthew Gooden and Gencho Rusev of LANL for valuable comments on the HI γ S experimental data, and Nathan Gibson for encouraging this work. This work was partially supported by the Office of Defense Nuclear Nonproliferation Research & Development (DNN R&D), National Nuclear Security Administration, U.S. Department of Energy. We gratefully acknowledge partial support by the Advanced Simulation and Computing (ASC) Program. This work was carried out under the auspices of the National Nuclear Security Administration of the U.S. Department of Energy at Los Alamos National Laboratory under Contract No. 89233218CNA000001.

-
- [1] J. B. Wilhelmy, E. Cheifetz, R. C. Jared, S. G. Thompson, H. R. Bowman, and J. O. Rasmussen, Angular momentum of primary products formed in the spontaneous fission of ^{252}Cf , *Phys. Rev. C* **5**, 2041 (1972).
- [2] L. Bonneau, P. Quentin, and I. N. Mikhailov, Scission configurations and their implication in fission-fragment angular momenta, *Phys. Rev. C* **75**, 064313 (2007).
- [3] I. Stetcu, P. Talou, T. Kawano, and M. Jandel, Isomer production ratios and the angular momentum distribution of fission fragments, *Phys. Rev. C* **88**, 044603 (2013).
- [4] G. F. Bertsch, T. Kawano, and L. M. Robledo, Angular momentum of fission fragments, *Phys. Rev. C* **99**, 034603 (2019).
- [5] J. N. Wilson, D. Thisse, M. Lebois, N. Jovančević, D. Gjestvang, R. Canavan, M. Rudigier, D. Étasse, R.-B. Gerst, L. Gaudefroy, E. Adamska, P. Adsley, A. Algora, M. Babo, K. Belvedere, J. Benito, G. Benzoni, A. Blazhev, A. Boso, S. Bottoni, M. Bunce, R. Chakma, N. Cieplicka-Oryńczak, S. Courtin, M. L. Cortés, P. Davies, C. Delafosse, M. Fallot, B. Fornal, L. Fraille, A. Gottardo, V. Guadilla, G. Häfner, K. Hauschild, M. Heine, C. Henrich, I. Homm, F. Ibrahim, L. W. Iskra, P. Ivanov, S. Jazrawi, A. Korgul, P. Koseoglou, T. Kröll, T. Kurtukian-Nieto, L. Le Meur, S. Leoni, J. Ljungvall, A. Lopez-Martens, R. Lozeva, I. Matea, K. Miernik, J. Nemer, S. Oberstedt, W. Paulsen, M. Piersa, Y. Popovitch, C. Porzio, L. Qi, D. Ralet, P. H. Regan, K. Rezykina, V. Sánchez-Tembleque, S. Siem, C. Schmitt, P.-A. Söderström, C. Sürder, G. Tocabens, V. Vedia, D. Verney, N. Warr, B. Wasilewska, J. Wiederhold, M. Yavahchova, F. Zeiser, and S. Ziliani, Angular momentum generation in nuclear fission, *Nature* **590**, 566 (2021).
- [6] P. Marević, N. Schunck, J. Randrup, and R. Vogt, Angular momentum of fission fragments from microscopic theory, *Phys. Rev. C* **104**, L021601 (2021).
- [7] I. Stetcu, A. E. Lovell, P. Talou, T. Kawano, S. Marin, S. A. Pozzi, and A. Bulgac, Angular momentum removal by neutron and γ -ray emissions during fission fragment decays, *Phys. Rev. Lett.* **127**, 222502 (2021).
- [8] A. Bulgac, I. Abdurrahman, S. Jin, K. Godbey, N. Schunck, and I. Stetcu, Fission fragment intrinsic spins and their correlations, *Phys. Rev. Lett.* **126**, 142502 (2021).
- [9] A. Bulgac, I. Abdurrahman, K. Godbey, and I. Stetcu, Fragment intrinsic spins and fragments' relative orbital angular momentum in nuclear fission, *Phys. Rev. Lett.* **128**, 022501 (2022).
- [10] B. Becker, P. Talou, T. Kawano, Y. Danon, and I. Stetcu, Monte Carlo Hauser-Feshbach predictions of prompt fission γ rays: Application to $n_{\text{th}} + ^{235}\text{U}$, $n_{\text{th}} + ^{239}\text{Pu}$, and $^{252}\text{Cf}(\text{sf})$, *Phys. Rev. C* **87**, 014617 (2013).
- [11] O. Litaize and O. Serot, Investigation of phenomenological models for the Monte Carlo simulation of the prompt fission neutron and γ emission, *Phys. Rev. C* **82**, 054616 (2010).
- [12] D. Regnier, O. Litaize, and O. Serot, An improved numerical method to compute neutron/gamma deexcitation cascades starting from a high spin state, *Computer Physics Communications* **201**, 19 (2016).
- [13] P. Talou, R. Vogt, J. Randrup, M. E. Rising, S. A. Pozzi, L. Nakae, M. T. Andrews, S. D. Clarke, P. Jaffke, M. Jandel, T. Kawano, M. J. Marcat, K. Meierbachtol, G. Rusev, A. Sood, I. Stetcu, J. Verbeke, and C. Walker, Correlated prompt fission data in transport simulations, *European Physical Journal* **54**, 9 (2018).
- [14] S. Okumura, T. Kawano, P. Jaffke, P. Talou, and S. Chiba, $^{235}\text{U}(n,f)$ independent fission product yield and isomeric ratio calculated with the statistical Hauser-Feshbach theory, *Journal of Nuclear Science and Technology* **55**, 1009 (2018).
- [15] P. Talou, I. Stetcu, P. Jaffke, M. Rising, A. Lovell, and T. Kawano, Fission fragment decay simulations with the CGMF code, *Computer Physics Communications* **269**, 108087 (2021).
- [16] A. Lovell, T. Kawano, S. Okumura, I. Stetcu, M. Mumpower, and P. Talou, Extension of the Hauser-Feshbach fission fragment decay model to multi-chance fission, *Phys. Rev. C* **103**, 014615 (2021).
- [17] S. Okumura, T. Kawano, A. Lovell, and T. Yoshida, Energy dependent calculations of fission product, prompt,

- and delayed neutron yields for neutron induced fission on ^{235}U , ^{238}U , and ^{239}Pu , *Journal of Nuclear Science and Technology* **59**, 96 (2022).
- [18] W. Hauser and H. Feshbach, The inelastic scattering of neutrons, *Phys. Rev.* **87**, 366 (1952).
- [19] T. Kawano, Unified description of the coupled-channels and statistical hauser-feshbach nuclear reaction theories for low energy neutron incident reactions, *European Physical Journal A* **57**, 16 (2021).
- [20] J. A. Silano and H. J. Karwowski, Near-barrier photofission in ^{232}Th and ^{238}U , *Phys. Rev. C* **98**, 054609 (2018).
- [21] T. Kawano, CoH₃: The coupled-channels and hauser-feshbach code, *Springer Proceedings in Physics* **254**, 27 (2021), CNR2018: International Workshop on Compound Nucleus and Related Topics, LBNL, Berkeley, CA, USA, September 24 – 28, 2018, J. Escher, Y. Alhassid, L.A. Bernstein, D. Brown, C. Fröhlich, P. Talou, W. Younes (Eds.).
- [22] J. L. Ullmann, T. Kawano, T. A. Bredeweg, A. Couture, R. C. Haight, M. Jandel, J. M. O'Donnell, R. S. Rundberg, D. J. Vieira, J. B. Wilhelmy, J. A. Becker, A. Chyzh, C. Y. Wu, B. Baramsai, G. E. Mitchell, and M. Krtička, Cross section and γ -ray spectra for $^{238}\text{U}(n,\gamma)$ measured with the DANCE detector array at the Los Alamos Neutron Science Center, *Phys. Rev. C* **89**, 034603 (2014).
- [23] M. Guttormsen, L. A. Bernstein, A. Görgen, B. Jurado, S. Siem, M. Aiche, Q. Ducasse, F. Giacoppo, F. Gunsing, T. W. Hagen, A. C. Larsen, M. Lebois, B. Leniau, T. Renström, S. J. Rose, T. G. Tornyi, G. M. Tveten, M. Wiedeking, and J. N. Wilson, Scissors resonance in the quasicontinuum of Th, Pa, and U isotopes, *Phys. Rev. C* **89**, 014302 (2014).
- [24] M. R. Mumpower, T. Kawano, J. L. Ullmann, M. Krtička, and T. M. Sprouse, Estimation of $m1$ scissors mode strength for deformed nuclei in the medium- to heavy-mass region by statistical hauser-feshbach model calculations, *Phys. Rev. C* **96**, 024612 (2017).
- [25] E. S. Soukhovitskii, R. Capote, J. M. Quesada, and S. Chiba, Dispersive coupled-channel analysis of nucleon scattering from ^{232}Th up to 200 MeV, *Phys. Rev. C* **72**, 024604 (2005).
- [26] T. Nakatsukasa, T. Inakura, and K. Yabana, Finite amplitude method for the solution of the random-phase approximation, *Phys. Rev. C* **76**, 024318 (2007).
- [27] H. Sasaki, T. Kawano, and I. Stetcu, Noniterative finite amplitude methods for $E1$ and $M1$ giant resonances, *Phys. Rev. C* **105**, 044311 (2022).
- [28] H. Sasaki, T. Kawano, and I. Stetcu, *QRPA calculations for M1 transitions with the noniterative finite amplitude method and the application to neutron radiative capture cross sections* (2022), submitted to *Phys. Rev. C*.
- [29] L. Bonneau, P. Quentin, and D. Samsøen, Fission barriers of heavy nuclei within a microscopic approach, *Eur. Phys. J. A* **21**, 391 (2004).
- [30] J. Kopecky and M. Uhl, Test of gamma-ray strength functions in nuclear reaction model calculations, *Phys. Rev. C* **41**, 1941 (1990).
- [31] A. Gilbert and A. G. W. Cameron, A composite nuclear-level density formula with shell corrections, *Can. J. Phys.* **43**, 1446 (1965).
- [32] T. Kawano, P. Talou, I. Stetcu, and M. B. Chadwick, Statistical and evaporation models for the neutron emission energy spectrum in the center-of-mass system from fission fragments, *Nuclear Physics A* **913**, 51 (2013).
- [33] V. E. Viola, K. Kwiatkowski, and M. Walker, Systematics of fission fragment total kinetic energy release, *Phys. Rev. C* **31**, 1550 (1985).
- [34] T. Ohsawa, T. Horiguchi, and H. Hayashi, Multimodal analysis of prompt neutron spectra for $^{237}\text{Np}(n,f)$, *Nuclear Physics A* **653**, 17 (1999).
- [35] A. C. Wahl, Nuclear-charge distribution and delayed-neutron yields for thermal-neutron-induced fission of ^{235}U , ^{233}U , and ^{239}Pu and for spontaneous fission of ^{252}Cf , *Atomic Data and Nuclear Data Tables* **39**, 1 (1988).
- [36] A. C. Wahl, *Systematics of Fission-Product Yields*, Tech. Rep. LA-13928 (Los Alamos National Laboratory, 2002).
- [37] F. Minato, Neutron energy dependence of delayed neutron yields and its assessments, *Journal of Nuclear Science and Technology* **55**, 1054 (2018).
- [38] D. A. Brown, M. B. Chadwick, R. Capote, A. C. Kahler, A. Trkov, M. W. Herman, A. A. Sonzogni, Y. Danon, A. D. Carlson, M. Dunn, D. L. Smith, G. M. Hale, G. Arbanas, R. Arcilla, C. R. Bates, B. Beck, B. Becker, F. Brown, R. J. Casperson, J. Conlin, D. E. Cullen, M. A. Descalle, R. Firestone, T. Gaines, K. H. Guber, A. I. Hawari, J. Holmes, T. D. Johnson, T. Kawano, B. C. Kiedrowski, A. J. Koning, S. Kopecky, L. Leal, J. P. Lestone, C. Lubitz, J. I. Márquez Damián, C. M. Mattoon, E. A. McCutchan, S. Mughabghab, P. Navratil, D. Neudecker, G. P. A. Nobre, G. Noguere, M. Paris, M. T. Pigni, A. J. Plompen, B. Pritychenko, V. G. Pronyaev, D. Roubtsov, D. Rochman, P. Romano, P. Schillebeeckx, S. Simakov, M. Sin, I. Sirakov, B. Sleaford, V. Sobes, E. S. Soukhovitskii, I. Stetcu, P. Talou, I. Thompson, S. van der Marck, L. Welter-Sherrill, D. Wiarda, M. White, J. L. Wormald, R. Q. Wright, M. Zerkle, G. Žerovnik, and Y. Zhu, ENDF/B-VIII.0: the 8th major release of the nuclear reaction data library with CIELO-project cross sections, new standards and thermal scattering data, *Nuclear Data Sheets* **148**, 1 (2018).
- [39] J. W. Meadows and C. Budtz-Jørgensen, *The fission fragment angular distributions and total kinetic energies for $^{235}\text{U}(n,f)$ from .18 to 8.83 MeV*, Tech. Rep. ANL/NDM-64 (Argonne National Laboratory, 1982).
- [40] C. M. Zoller, *Investigation of Neutron-Induced Fission of ^{238}U in the Energy Range from 1 MeV to 500 MeV*, Ph.D. thesis, Department of Physics, Technische Hochschule Darmstadt (1995).
- [41] N. Akimov, V. Vorobyeva, V. Kabenin, N. Kolosov, B. Kuzminov, A. Sergachev, L. Smirenkina, and M. Tarasko, Effect of excitation energy on yields and kinetic energies of fragments at the fission of Pu-239 by neutrons, *Yadernaya Fizika* **13**, 484 (1971).
- [42] V. G. Vorobeve, N. P. Dyachenko, N. P. Kolosov, B. D. Kuzminov, and A. Sergachev, Effect of nucleonic composition of fissioning nuclei on mean kinetic-energy of fragments, *Yadernaya Fizika* **19**, 954 (1974).
- [43] K. Meierbachtol, F. Tovesson, D. L. Duke, V. Geppert-Kleinrath, B. Manning, R. Meharchand, S. Mosby, and D. Shields, Total kinetic energy release in $^{239}\text{Pu}(n,f)$ post-neutron emission from 0.5 to 50 MeV incident neutron energy, *Phys. Rev. C* **94**, 034611 (2016).
- [44] D. Duke, *Fission fragment mass distributions and total kinetic energy release of $^{235}\text{-uranium}$ and $^{238}\text{-uranium}$ in neutron-induced fission at intermediate and fast neutron*

- energies, Ph.D. thesis, Colorado State University (2014).
- [45] D. L. Duke, F. Tovesson, A. B. Laptev, S. Mosby, F.-J. Hamsch, T. Brys, and M. Vidali, Fission-fragment properties in $^{238}\text{U}(n, f)$ between 1 and 30 MeV, *Phys. Rev. C* **94**, 054604 (2016).
- [46] J. T. Caldwell, G. M. Worth, and E. J. Dowdy, Prompt and delayed neutrons from low energy photo-reactions Part II: simultaneous measurement of prompt ν , Γ_n/Γ_f , and delayed neutrons per fission for ^{232}Th , ^{235}U , ^{238}U , and ^{239}Pu for 8-, 10- and 12-MeV bremsstrahlung (1973) p. 651, int. Conf. on Photonuclear Reactions and Applications, Pacific Grove, California, USA.
- [47] J. T. Caldwell and E. J. Dowdy, Experimental determination of photofission neutron multiplicities for eight isotopes in the mass range $232 \leq A \leq 239$, *Nuclear Science and Engineering* **56**, 179 (1975).
- [48] J. T. Caldwell, E. J. Dowdy, R. A. Alvarez, B. L. Berman, and P. Meyer, Experimental Determination of Photofission Neutron Multiplicities for ^{235}U , ^{236}U , ^{238}U , and ^{232}Th Using Monoenergetic Photons, *Nuclear Science and Engineering* **73**, 153 (1980).
- [49] L. I. Prokhorova and G. N. Smirenkin, Mean number of prompt neutrons emitted in photo fission of ^{232}Th and ^{238}U γ -rays produced in the $^{19}\text{F}(p, \alpha \gamma)^{16}\text{O}$ reaction, *The Soviet Journal of Atomic Energy* **8**, 390 (1961).
- [50] A. M. Khan and J. W. Knowles, Photofission of ^{232}Th , ^{238}U and ^{235}U near threshold using a variable energy beam of γ -rays, *Nuclear Physics A* **179**, 333 (1972).
- [51] B. L. Berman, J. T. Caldwell, E. J. Dowdy, S. S. Dietrich, P. Meyer, and R. A. Alvarez, Photofission and photoneutron cross sections and photofission neutron multiplicities for ^{233}U , ^{234}U , ^{237}Np , and ^{239}Pu , *Phys. Rev. C* **34**, 2201 (1986).
- [52] T. Kawano, Y. Cho, P. Dimitriou, D. Filipescu, N. Iwamoto, V. Plujko, X. Tao, H. Utsunomiya, V. Varlamov, R. Xu, R. Capote, I. Gheorghe, O. Gorbachenko, Y. Jin, T. Renstrøm, M. Sin, K. Stopani, Y. Tian, G. Tveten, J. Wang, T. Belgya, R. Firestone, S. Goriely, J. Kopecky, M. Krτίčka, R. Schwengner, S. Siem, and M. Wiedeking, IAEA Photonuclear Data Library 2019, *Nuclear Data Sheets* **163**, 109 (2020).
- [53] N. Iwamoto, K. Kosako, and T. Murata, Photonuclear data file, *JAEA-Conf* **2016-004**, 53 (2016), proceedings of the 2015 Symposium on Nuclear Data, November 19–20, 2015, Ibaraki Quantum Beam Research Center, Tokai-mura, Ibaraki, Japan.
- [54] A. De Clercq, E. Jacobs, D. De Frenne, H. Thierens, P. D’hondt, and A. J. Deruytter, Fragment mass and kinetic energy distribution for the photofission of ^{235}U and ^{238}U with 25-MeV end-point bremsstrahlung, *Phys. Rev. C* **13**, 1536 (1976).
- [55] P. Talou, T. Kawano, I. Stetcu, J. P. Lestone, E. McKigney, and M. B. Chadwick, Late-time emission of prompt fission γ rays, *Phys. Rev. C* **94**, 064613 (2016).
- [56] I. Stetcu, P. Talou, T. Kawano, and M. Jandel, Properties of prompt-fission γ rays, *Phys. Rev. C* **90**, 024617 (2014).
- [57] H. Makii, K. Nishio, K. Hirose, R. Orlandi, R. Léguillon, T. Ogawa, T. Soldner, U. Köster, A. Pollitt, F.-J. Hamsch, I. Tsekhanovich, M. Aiche, S. Czajkowski, L. Mathieu, C. M. Petrache, A. Astier, S. Guo, T. Ohtsuki, S. Sekimoto, K. Takamiya, R. J. W. Frost, and T. Kawano, Effects of the nuclear structure of fission fragments on the high-energy prompt fission γ -ray spectrum in $^{235}\text{U}(n_{\text{th}}, f)$, *Phys. Rev. C* **100**, 044610 (2019).
- [58] Krishichayan, M. Bhihe, C. R. Howell, A. P. Tonchev, and W. Tornow, Fission product yield measurements using monoenergetic photon beams, *Phys. Rev. C* **100**, 014608 (2019).
- [59] H. Thierens, D. De Frenne, E. Jacobs, A. De Clercq, P. D’hondt, and A. J. Deruytter, Product yields for the photofission of ^{235}U and ^{238}U with 25-MeV bremsstrahlung, *Phys. Rev. C* **14**, 1058 (1976).
- [60] D. Doré, J.-C. David, V. Macary, J.-M. Laborie, X. Ledoux, D. Ridikas, and A. Vanlauwe, Delayed neutron yields and spectra from photofission of actinides: data and calculations with Bremsstrahlung photons below 20 MeV, *EPJ Web of Conferences* , 335 (2008), proc. Int. Conf. on Nuclear Data for Science and Technology, 22 – 27 Apr., 2007, Nice, France, Ed. O. Bersillon, F. Gunsing, E. Bauge, R. Jacqmin, and S. Leray.
- [61] V. Macary, E. Berthoumieux, D. Doré, S. Panebianco, D. Ridikas, J.-M. Laborie, and X. Ledoux, Photofission of ^{235}U and ^{237}Np with bremsstrahlung photons below 20 MeV: measurements of delayed neutron yields and time spectra, *Nuclear Technology* **168**, 287 (2009).